J Mater Sci (2009) 44:492–501
DOI 10.1007/s10853-008-3097-9

Fluidity and microstructure of an Al–10% B_4C composite

Z. Zhang · X.-G. Chen · A. Charette

Received: 29 July 2008 / Accepted: 30 October 2008 / Published online: 23 November 2008

Abstract The fluidity evolution of an Al–10 vol.% B_4C experimental composite during long holding periods has been investigated by using a vacuum fluidity test. It was found that the fluidity of the composite melt decreased with the increase of the holding time. The microstructure of the fluidity samples was examined by optical metallography, quantitative image analysis, and electron microscopy. Two secondary reaction-induced phases were identified and the volume fraction changes of the solid phases during the holding periods were quantified. The relationship between the fluidity, volume fraction, and surface area of solid phase particles was established. In addition, the particle distribution along the entire length was examined in the fluidity samples. The mechanism of the particle redistribution during flow and solidification is presently discussed.

Introduction

Over the years, the manufacture of metal matrix composites (MMCs) has been consolidated into two main process routes: the liquid mixing process and the powder metallurgy process. The liquid mixing process has advantages over the powder metallurgy in terms of ease of production of large quantities at a lower cost [1]. This process is employed to produce most of the commercial Al-based metal–matrix composites such as Al–SiC, Al–Al_2O_3, and Al–B_4C MMCs [1, 2]. However, good fluidity is a basic requirement for the composites to be produced in the forms of DC and shape casting, as well as the recycling of these materials by the liquid mixing and casting process. The fluidity can be defined as the ability of molten metal to flow in a long channel of small cross sections [3]. The length the metal flows before it is stopped by solidification is the measure of fluidity. To evaluate the fluidity of metals, there are two common types of fluidity tests: the spiral fluidity and the vacuum fluidity tests [3, 4]. The fluidity of Al-based metal matrix composites has been studied by several researchers [5–8]. A theoretical model was proposed to describe the composite fluidity as seen in Eq. 1 [5].

$$L_f = \frac{(\rho_m \Phi_m + \rho_d \Phi_d) a v}{2h(T_m - T_o)} [H_m(1 - \Phi_d) + (C_m W_m + C_d W_d)\Delta T] \quad (1)$$

where L_f is the length of flow, or simply called fluidity, ρ, Φ, C, H, and W are the density, volume fraction, specific heat, latent heat, and weight fraction of the matrix (m) and reinforcement particles (d), respectively. The superheat is ΔT, and h is the heat-transfer coefficient at the mold–metal interface, a is the radius of the channel, v is the velocity of the molten metal, T_m is the metal melting point, and T_o is the mold temperature.

This equation predicts a decrease in fluidity with an increase in volume fraction of solid particles [6]. It also indicates that the density, fraction, and thermal properties of particles have an important effect on the fluidity. It should be noted that some factors affecting the composite fluidity such as settling, agglomeration and pushing of particles, presence of gas and oxides, and reaction-induced changes are not considered in this equation [6]. These variable conditions could result in a deviation between the theoretical and the experimental results.

However, it was also observed that the fluidity of the Al-based composites was related to the size and shape of

Z. Zhang (✉) · X.-G. Chen · A. Charette
Université du Québec à Chicoutimi, Chicoutimi, Canada G7H 2B1
e-mail: zhan_zhang@uqac.ca

reinforcing particles (Al_2O_3 and SiC) [7, 8]. The composite fluidity decreased with a decrease in particle size and with an increase of angularity for a given percentage of the reinforcement. The relationship between the fluidity length (F in cm) and the Al_2O_3 particle surface area (x in m^2/100 g) could be expressed by Eq. 2, where a and b are constants [7].

$$F = a - bx \tag{2}$$

It was suggested that the decrease in the Al–alumina composite fluidity with an increase of the surface area of alumina particles may be attributed to the viscosity increase in the melts [7].

As for the particle distribution in an AlSi7Mg–SiC composite, it was reported that the first 100 mm of the spirals (fluidity test samples) had an almost uniform particle distribution, but that further away from the entrance, the microstructure was dominated by round areas without particles [9]. Moreover, in a particle suspension system, fluid flow influences particle distribution [10]. The particles in the dispersion system move toward the center where shearing is at a minimum [10]. In addition, segregation bands were observed in high pressure or gravity die castings [11–15]. Dahle and St. John [16] proposed an explanation for this phenomenon. The formation of a segregation band relates to the mechanical behavior of the partially solidified microstructure when shear stresses develop during the filling of a cast part [13, 16].

Recently, the liquid mixing process has been adapted for producing castable Al–B_4C particulate reinforced composites for applications in the nuclear industry. These composites have superior mechanical properties, thermal conductivity, and are especially capable of capturing neutrons [2]. However, since there are strong interfacial reactions between B_4C and liquid aluminum, it would be difficult to use this process to produce Al–B_4C composites if the interfacial reactions could not be controlled [17–22]. It was reported that when the Al–B_4C temperature is between 660 °C and 868 °C, the reaction products are Al_3BC and AlB_2 [19]. To overcome the reactivity problem of B_4C particles, titanium is added into the composite melt to form a barrier layer on the surface of the B_4C particulate, thus limiting the interfacial reactions between the B_4C and liquid aluminum [15, 17, 18, 23]. However, quantitative information on the impact of solid particles on the fluidity evolution of molten Al–B_4C composites, including the reaction-induced second particles, has not yet been reported.

In this paper, the fluidity evolution of the experimental composite Al–10% B_4C containing 0.67% Ti was examined by using a vacuum fluidity test set-up during a long holding period. The relationship between the fluidity evolution and the formation of the microstructure, as well as the interfacial reaction products during the holding period, were investigated in order to understand the fluidity behavior of the composite. In addition, the particle distribution in the fluidity samples was analyzed and the results were interpreted.

Experimental procedure

Direct Chill (DC) cast billets of AA1100–15 vol.% B_4C, fabricated by Rio Tinto Alcan's Dubuc plant, were used to prepare the experimental composite for the fluidity testing. The average B_4C particle size was approximately 17 μm. During the batch operation, prefabricated B_4C billets and commercially pure aluminum, along with the Ti master alloy, were melted in an electric resistance furnace in such proportions that the final composite consisted of 10 vol.% B_4C and 0.67% Ti. The composite melt was held under mechanical stirring using an impeller to ensure a uniform distribution of B_4C particles in the liquid. The melt temperature was maintained at 730 ± 2 °C for approximately 15 h.

A vacuum fluidity test set-up (Fig. 1a) was used for the fluidity evaluation. In the fluidity tests, composite melt was

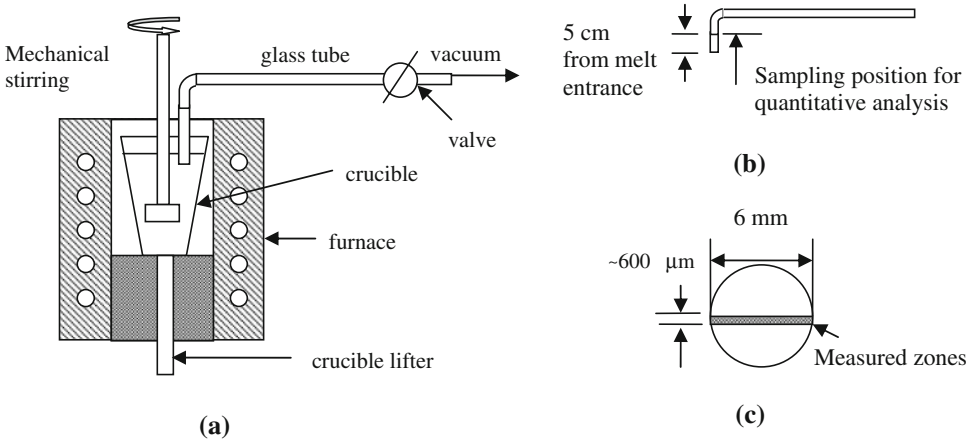

Fig. 1 **a** Set-up sketch of the vacuum fluidity test; **b** sampling position for quantitative analysis of solid particles; **c** quantitative analysis zone on a cross section of a sample

drawn into a 6 mm inside diameter glass tube under the predetermined 215 mmHg pressure. While taking the fluidity samples, the tubes were immersed into the melt approximately 25 mm deep. A crucible lifter was used to maintain a constant immersion depth of the glass tube in the melt. Fluidity samples were regularly taken at intervals of 20–60 min. After solidification of the composite in the glass tube, the length of the composite in the tube (length of flow) was measured for the fluidity evaluation. Some fluidity samples were sectioned (longitudinally or transversely) at different positions for microstructural examination.

An optical image analyzer (CLEMEX JS-2000, PE4.0) was used to quantitatively measure the volume fraction of B_4C particles and its reaction products at a 500× magnification. The sampling position and the measured zone for the quantitative measurement are shown in Fig. 1b and c. An electron probe microanalyzer (EPMA, CAMECA SX-100) equipped with a wavelength dispersive spectrometer (WDS) was used to examine the chemical compositions of different compounds in the composite. Five measurements were carried out for each compound. The transmission electron microscope (JEM 2100F) was used for the determination of the crystal structure of the reaction products.

Results and discussion

Fluidity evolution

Figure 2 shows the fluidity evolution of the composite during the holding time. The fluidity of the composite declines with the increase of the holding time. However, the fluidity decline is not constant. In the first stage, the fluidity decreases from 73 to 30 cm (holding times up to 400 min) which represents approximately 80% of the total fluidity decrease. After this period, the variation of fluidity is only between 30 and 22 cm. A continuous decrease of fluidity indicates that the rheological properties of the composite melt have significantly changed during the holding time.

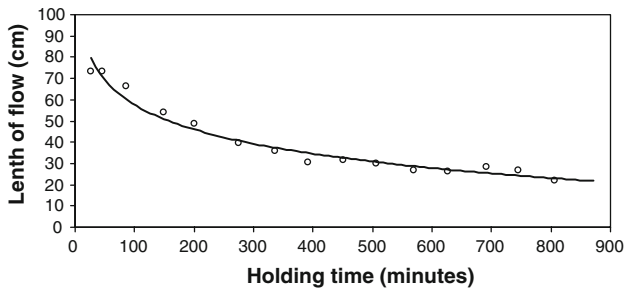

Fig. 2 Fluidity evolution during the holding time

Microstructure

Figure 3 shows the optical metallographs of samples with 25, 400, and 750 min holding times. The 25 min sample represents the initial microstructure after remelting. The 400 min sample shows the microstructure of the composite at the end of the first holding stage, while the 750 min sample is an example of the microstructure after a long holding time. In these micrographs, secondary reaction-induced solid particles around the B_4C particles appear in the aluminum matrix. These particles are the interfacial reaction products. The color of one type of the particle is yellow and that of the other one is gray under the optical microscope. Most of the gray particles are connected or close to the B_4C particles. The yellow particles are often not attached to B_4C particles. From Fig. 3 it can be clearly seen that, with an increased holding time, the amount and size of the two types of reaction-induced particles increase significantly.

Several yellow particles were examined using an electron probe microanalyzer (EPMA). The analyzed chemical compositions were compared to the stoichiometrical composition of the AlB_2 phase (Table 1). Based on the result, it was identified that the yellow particles appearing under the optical microscope were AlB_2.

The EPMA backscattered electron image of the 750 min holding time sample is shown in Fig. 4. A Ti-rich layer enclosing B_4C particles and some reaction product particles distributed inside and outside of this layer were found. The reaction product particles consist of Al, B, and C elements detected by EPMA. However, the size of these particles is too small to obtain quantitative data. The transmission electron microscope was used to determine the crystal structure of the phases in the samples. The data from the electron diffraction patterns in the selected area on these phases show that the Ti-rich layer is composed of fine TiB_2 crystals (crystal size: 0.1–0.5 μm) and that the reaction products are Al_3BC crystals (crystal size: 0.3–0.8 μm). Figure 5 is a TEM dark field image of the sample with a long holding time (750 min). In this micrograph, there are two B_4C particles. The smaller one is located at the lower right corner. In B_4C surfaces, there is a layer of Al_3BC crystals and then a layer of fine TiB_2 crystals that encloses the Al_3BC layer and the B_4C particles. Outside the TiB_2 layer, there is another layer of Al_3BC crystals which continues to grow during the holding period. Therefore, the gray particles seen in the optical metallographs include two phases: TiB_2 and Al_3BC.

Based on the above observation, the microstructure of the composite consists of B_4C particles and phases Al_3BC, AlB_2, and TiB_2. The addition of Ti during remelting reacts with B_4C to form a TiB_2 layer around the B_4C particles.

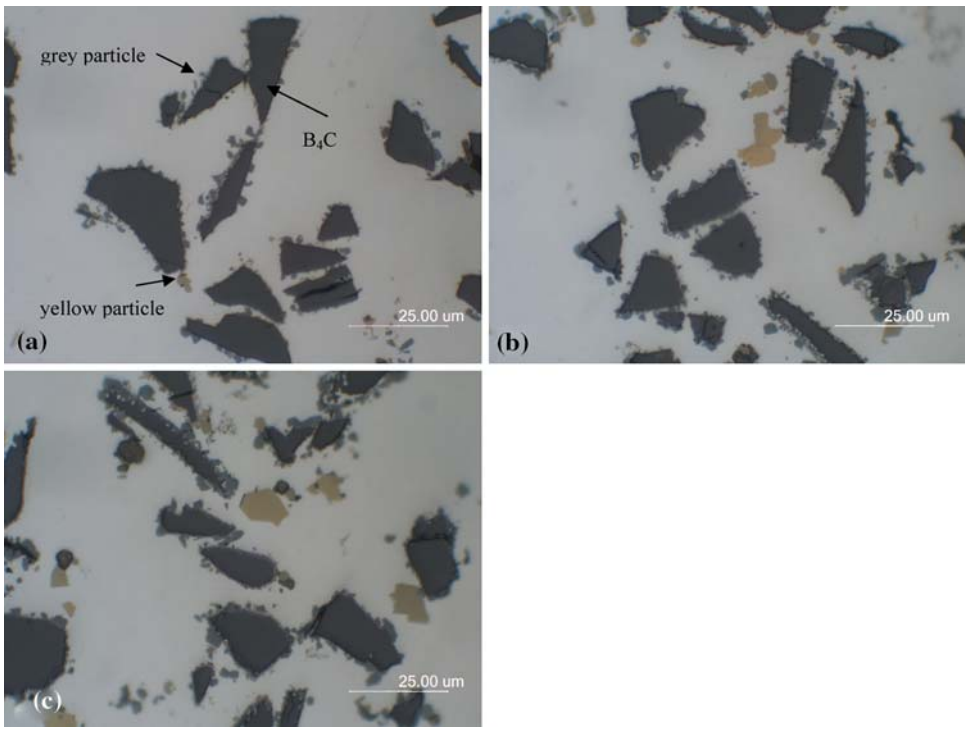

Fig. 3 Microstructures of the fluidity test samples with: **a** 25 min holding time, **b** 400 min holding time, and **c** 750 min holding time

Table 1 Chemical compositions of the yellow phase (at.%)

Phase	Analyzed composition		Stoichiometrical composition of AlB_2	
	Al	B	Al	B
Yellow particles	34.3 (1.0)[a]	65.7 (1.2)[a]	33.3	66.7

[a] The standard deviation of the analysis is given in parenthesis

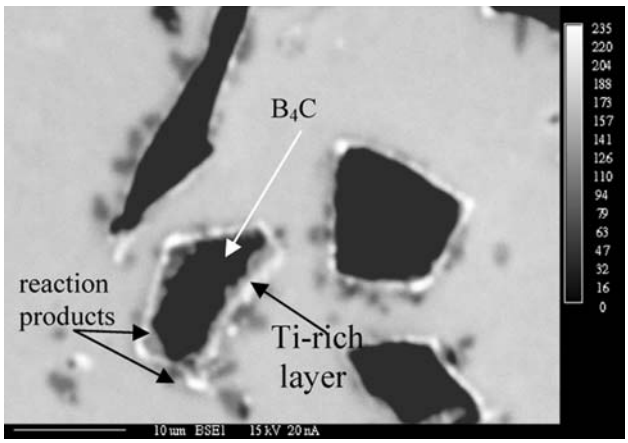

Fig. 4 Backscattered electron image of the fluidity test sample with 750 min holding time

During holding, B_4C decomposes to form secondary reaction phases Al_3BC and AlB_2 as seen in Eq. 3

$$9Al + 2B_4C = 2Al_3BC + 3AlB_2 \quad (3)$$

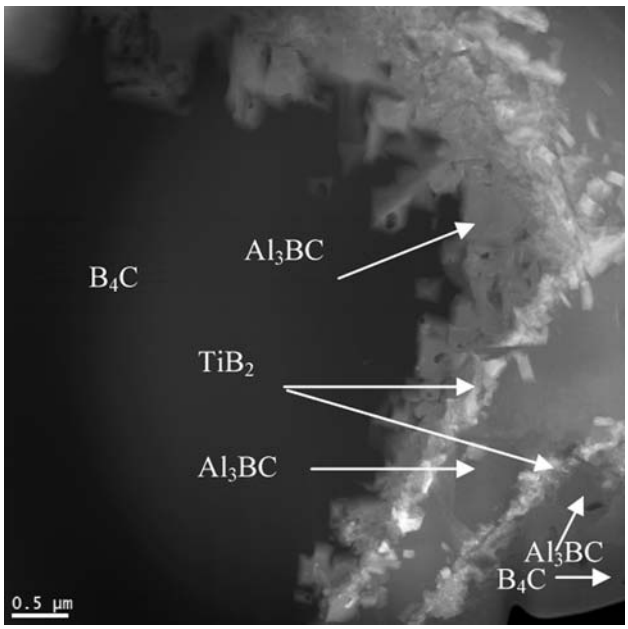

Fig. 5 A dark field image (TEM) of the sample with 750 min holding time

These reactions and their reaction products (Al_3BC, TiB_2, and AlB_2) have also been confirmed in other B_4C systems such as Al–Si–B_4C composites and Al–B_4C couples [15, 19, 24]. It is clear that the amount of reaction products changes while the type of reaction phases remains the same during the holding time in the fluidity test.

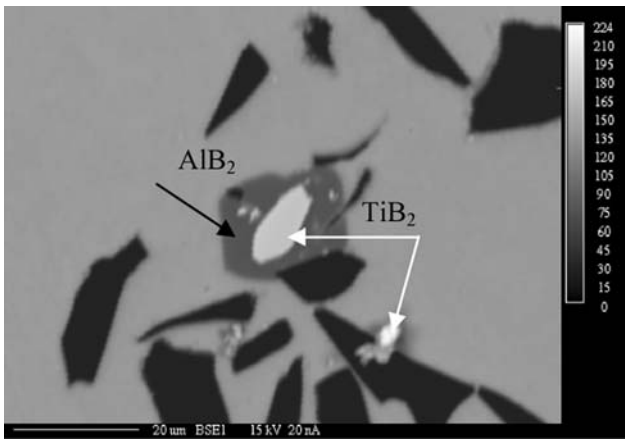

Fig. 6 Backscattered electron image showing AlB_2 formed on TiB_2 crystals

Table 2 Crystallographic data for TiB_2 and AlB_2

Compound	Crystal system	a (Å)	b (Å)	c (Å)
AlB_2	Hexagonal	3.0090	3.0090	3.2620
TiB_2	Hexagonal	3.0303	3.0303	3.2295

It is also interesting to note that AlB_2 crystals could nucleate and grow on TiB_2 particles (Fig. 6). The titanium boride can be obtained from the reaction-induced TiB_2 particles or from grain refiners (TiB_2) in commercial aluminum ingots. TiB_2 belongs to the same crystal system as AlB_2, i.e. hexagonal. The lattice parameters of TiB_2 and AlB_2 crystals are very similar and the difference is less than 1% (Table 2).

Quantitative analysis of B_4C and reaction-induced particles

Figure 7 shows the volume fraction changes of B_4C particles and reaction products as a function of the holding time. Here, the fractions of Al_3BC and TiB_2 were measured as a whole as it was difficult to distinguish the gray grades between Al_3BC and TiB_2 under the optical image analyzer. It should be mentioned that TiB_2 was formed during remelting. As Ti was no longer available in the matrix after remelting, the amount of TiB_2 remained constant during the composite melt holding. Therefore, increase of the Al_3BC and TiB_2 fractions can be considered as the net volume increase of Al_3BC. The Al_3BC and TiB_2 fraction at the 25 min holding time is 3.3 vol.% in the composite. After a long holding time (850 min), this volume fraction reaches 6.5 vol.%. On the other hand, the AlB_2 fraction also increases when prolonging the holding time. Its fraction is 0.2 vol.% at 25 min holding time and reaches 1.8 vol.% at 850 min holding time. Consequently, the total volume fraction of the reaction products increases from 3.5 to 8.3% during the long time holding. However, the fraction of B_4C decreases from 9.5% at 25 min holding time to 7.6% at 850 min holding time due to its decomposition. It is evident that, while the volume fraction of B_4C decreases slowly with the increased holding time, the volume fraction of the reaction products increases significantly.

Figure 8 indicates the volume fraction of the total solid particles (B_4C, Al_3BC, TiB_2, and AlB_2) in the composite as a function of the holding time. The volume fraction of the solid particles is approximately 13% at 25 min holding time and reaches 16% after holding 850 min. It is clear that the volume fraction of total solid particles increases with the holding time. The volume fraction growth of Al_3BC and AlB_2 contributes to this increase. Table 3 lists some chemical and physical properties of the solid particles found in Al–B_4C composites. Upon decomposition of a B_4C mole, one Al_3BC mole and 1.5 AlB_2 mole are formed. The resulting volume of Al_3BC and AlB_2 is 2.7 times that of B_4C.

As the secondary reaction phases Al_3BC and AlB_2 continue to grow around B_4C particles during holding, the surface of B_4C particles becomes more irregular and rough (Fig. 3). The surface area of the particles expands heavily besides the volume increase of the solid particles. Figure 9 gives the relationship between the surface area (S_v) of the total solid particles per unit volume and the melt holding time. The surface area at the 25 min holding time is approximately 7.5×10^{-2} m^2/cm^3. However, it reaches

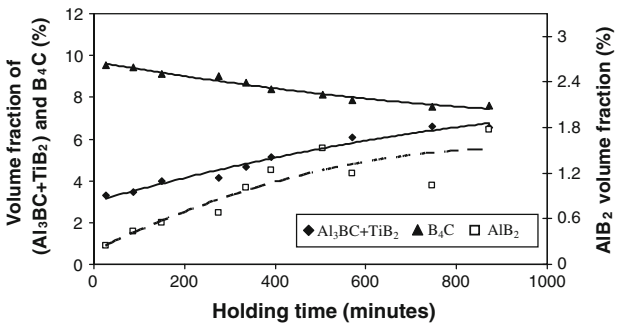

Fig. 7 Volume fraction of reaction products and B_4C particles as a function of the holding time

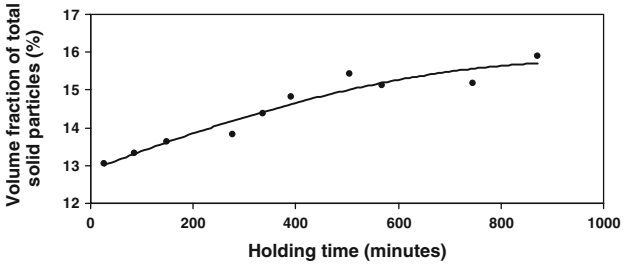

Fig. 8 Volume fraction of total solid particles as a function of the holding time

Table 3 Chemical and physical data of solid particles in Al–B_4C composites

Type of particles	Amount of atomic boron	Molar mass (g/mole)	Density (g/cm^3)	Molar volume (cm^3/mole)
B_4C	4	55.25	2.52	21.92
Al_3BC	1	103.77	2.85	36.41
AlB_2	2	48.60	3.16	15.38
TiB_2	2	69.52	4.49	15.48

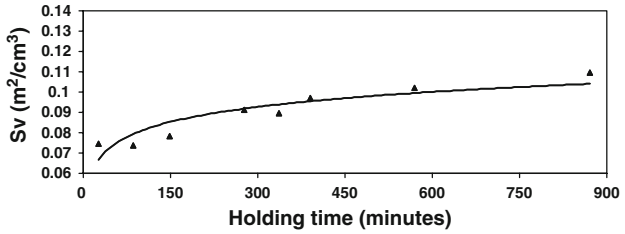

Fig. 9 Surface area of solid particles in Al–10 vol.% B_4C

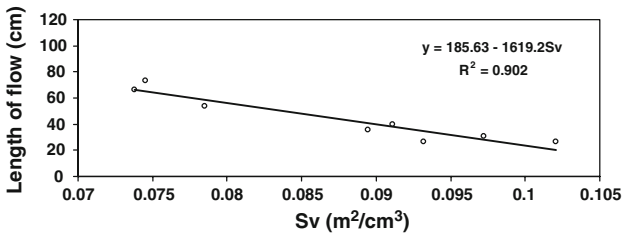

Fig. 10 Length of flow as a function of surface area in Al–10 vol.% B_4C

11.0×10^{-2} m^2/cm^3 after holding 850 min which is 1.5 times that of the former. This increase is due to the small size and angular shapes of the increased reaction products. Figure 10 shows the length of flow as a function of the surface area of the total solid particles. The flow length decreases with the increase of the surface area of the solid particles. A regression analysis indicates that the flow length correlates linearly with the surface area as the empirical Eq. 4

$$L_f = 185.63 - 1619.2\, S_v \text{ with a correction coefficient} = 0.902 \quad (4)$$

where L_f is the length of the flow (cm) and S_v is the surface area of the total separated solid particles per unit volume (m^2/cm^3). The surface area of solid particles S_v was determined by using Eq. 5 [25]

$$S_v = \frac{4}{\pi} \cdot L_A \quad (5)$$

where L_A is the population average value of the total perimeters of solid particles per unit area.

Based on the above microstructural observation and quantitative analysis of the solid particles in the composite, the evolution of the composite microstructure and its influence on the fluidity could be summarized as follows. As titanium is added into the melt, a barrier layer of TiB_2 crystals on the B_4C surface forms to limit the interfacial reactions between B_4C and Al [2, 15, 17, 18, 23]. However, liquid aluminum is still able to penetrate the barrier to react with B_4C particles. During a long holding time, the surface of B_4C particles becomes more irregular and rough while the secondary reaction phases Al_3BC and AlB_2 continue to grow. This results in the large increase of the surface area of the solid particles in the composite. With further increases in holding time, the ratio of the surface area increase slows down. This is probably due to the increased particle size. Therefore, the surface area increases faster in the first holding stage (up to 400 min) than in the remaining holding time (Fig. 9). On the other hand, the increased surface area increases the viscosity of the melt [7, 9], which results in the decline of the fluidity of the composite melt. Therefore, the flow length decreases with the increase of the holding time due to the increase of the solid particles and their surface area. Moreover, the fluidity decreases faster at the first holding stage than at the remaining holding time because of the faster increase of the surface area at this stage.

It should be mentioned that there are other factors impacting the fluidity of the composite in flowing process such as solid particle clusters, networks, and particle redistribution. These factors could affect the resistance of fluid flow in the fluidity tests. More details are discussed below.

Particle distribution during flow and solidification

Figure 11 shows an entire sample of the vacuum fluidity test. Several samples at various holding times were sectioned longitudinally and the microstructures were examined at different locations along the length to understand the particle distribution during the flow. It was observed that, although all solid particles have been carried in the long channel by the melt, the distribution of B_4C and the reaction particles is far from homogeneous. Figure 12 gives an example of such samples at typically three locations.

Generally, the particle distribution near the melt entrance is more or less uniform (Fig. 12a). The average

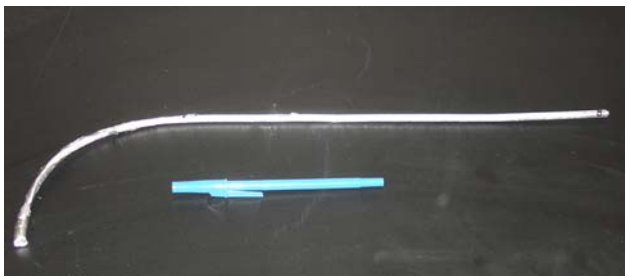

Fig. 11 A fluidity test sample

volume fraction of B_4C particles is approximately 9.5%, which is close to the designed fraction of B_4C particles in the composite (Table 4). As the flow continues along the channel, segregation bands appear near the glass tube wall. These can be seen in the middle of the sample (Fig. 12b). A few particles are present in these bands and more particles concentrate toward the center of the cross section. As the melt slurry goes further, there is an enrichment of the solid particles toward the flow end (Fig. 12c). The average volume fraction of B_4C at the end reaches 19.6 % and the volume fraction of the total solid particle fraction is 27.9%, which is twice as much as the volume fraction of B_4C and the total solid particles near the melt entrance (Table 4).

Table 4 Volume fraction of solid particles

Solid particle	Average volume fraction of solid particle (%)	
	Near entrance	End
B_4C	9.5	19.6
Total solid particles	13.3	27.9

In a particle suspension system, fluid flow affects the particle distribution [10]. The particles in the system move

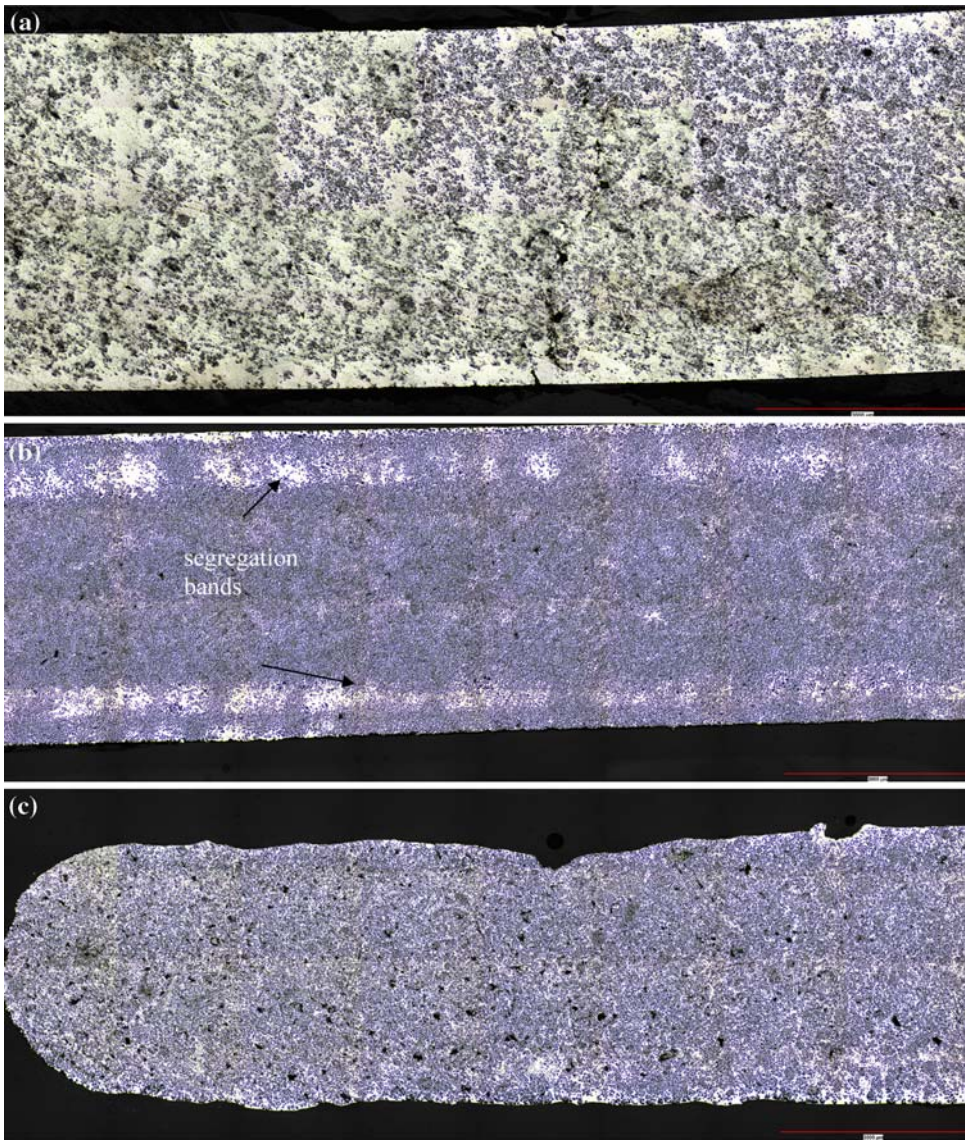

Fig. 12 Particle distribution in a sample with a 45 min holding time; the melt flow is from right to left: **a** a section near the melt entrance (3–18 mm away from the melt entrance); **b** near the sample middle (375–391 mm); **c** at the end of the sample (715–730 mm)

toward the center where shearing is at the minimum [10]. Combining the formation of particle segregation and the effect of fluid flow on a particle suspension system [10, 16], the particle redistribution process in the composite could be described as follows. When a solidified layer is formed on the tube wall and composite melt flows on the layer, a shear force arises between the solidified layer and the melt flow. Under the shear forcing, liquid aluminum concentrates on the interface (solidified layer/composite melt) and acts as a lubricant to reduce the flow resistance and consequently results in the formation of the segregation bands and the concentration of solid particles in the center and at the end. Figure 13 is a schematic diagram of the particle migration process. The particle migration results in a higher than average volume percentage of solid particles at the center and at the end of the samples. This higher particle volume in the flow centers and ends decreases the flow length in the fluidity tests due to the higher viscosity for the melt with a higher solid particle volume.

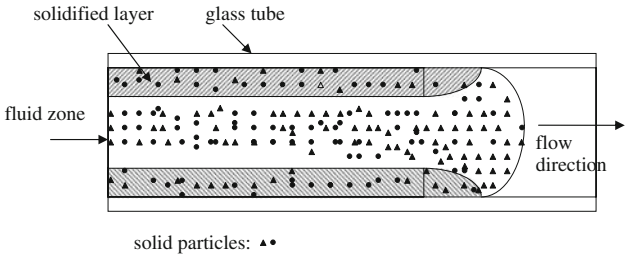

Fig. 13 Schematic diagram of the migration of solid particles

On the other hand, particle agglomerates such as particle clusters and particle networks were observed in the fluidity samples. Particle cluster is one type of particle agglomerate, forming a dense solid particle complex (Fig. 14a). Particle network is a less dense agglomerate where large particles (B_4C) are joined by small reaction-induced particles (Fig. 14b, c). These agglomerates are formed during the composite preparation and melt holding. They move as a whole during fluid flowing and occupy a much greater space in fluid flowing than the solid particles when they are separated. Consequently, the apparent volume of solid particles is remarkably increased due to these agglomerates. Moreover, particle clusters and networks increased with the holding time due to the increase of the reaction products during melt holding. Furthermore, it was found that most of the particle clusters and particle networks concentrated at the center and at the end of fluidity test samples (Figs. 14 and 15). This could be due to the actions combining the pushing by solid/liquid growth interface [8, 12] and the solid particle migration. The concentration of the agglomerates results in an increase of the flow resistance to the composite melt during the fluidity tests. It is evident that the particle clusters and networks in the fluidity test samples deteriorate the fluidity of the composite.

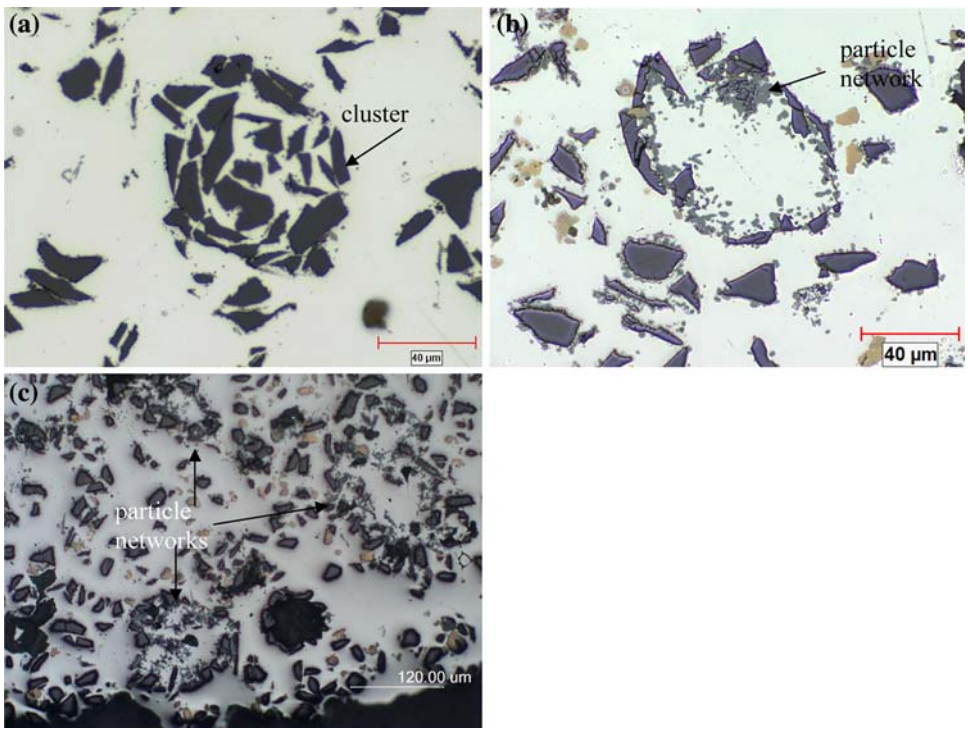

Fig. 14 Particle cluster and network: **a** particle cluster at the center of the sample with a 25 min holding time; **b** particle network at the center of the sample with a 450 min holding time; **c** particle networks at the end of the sample with a 750 min holding time

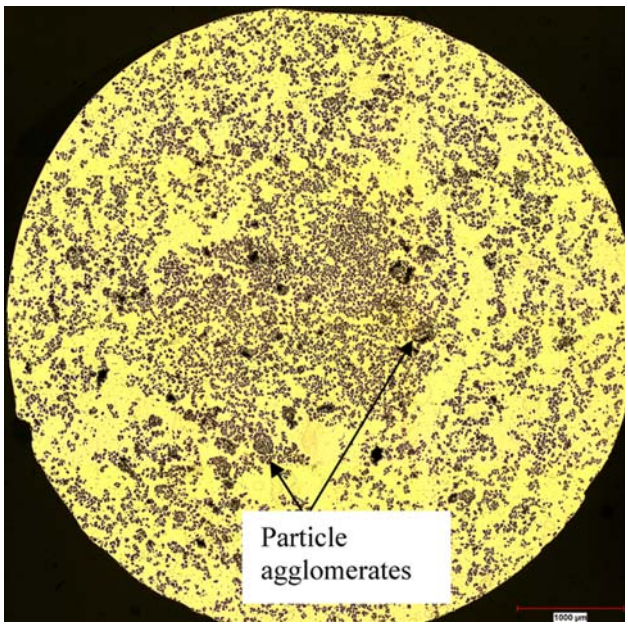

Fig. 15 Particle agglomerate distribution in a cross section of the sample with 25 min holding at 190 mm away from the melt entrance

Conclusions

Based on the above observations and discussions on the experimental composite Al–10% B_4C containing 0.67% Ti, the following conclusions are summarized.

1. The fluidity of Al–10% B_4C decreases with the increase of the holing time, and during the first period of holding time (up to 400 min), the deterioration of fluidity is faster than the rest.
2. The microstructure of the composite consists of B_4C particles and phases Al_3BC, AlB_2, and TiB_2. The addition of Ti during remelting reacts with B_4C to form a TiB_2 layer around the B_4C particles. During remelting and long holding periods, B_4C decomposes to form two secondary reaction phases Al_3BC and AlB_2 due to the interfacial reaction between B_4C and liquid aluminum.
3. When increasing the holding time, the volume fraction of B_4C decreases moderately, while the volume fraction of reaction phases increases significantly. This leads to the increase of the solid particle volume and the large increase of the particle surface area in the composite melt. The increase of the total surface area and the volume fraction of solid particles results in the decline of the fluidity.
4. The particle clusters and networks have an important contribution to the deterioration of the composite fluidity.
5. During the melt flow in the long channel, solid particles redistribute along the path. Segregation and enrichment of solid particles toward the section center and flow direction are observed. The average volume fraction of particles at the flow end is much higher than that near the melt entrance. The mechanism of the particle redistribution in the metal matrix composites during flow and solidification is discussed.

Acknowledgements The authors would like to acknowledge the financial support of the Natural Sciences and Engineering Research Council of Canada (NSERC) and Rio Tinto Alcan Inc., Arvida Research and Development Centre (ARDC). They are also grateful to A. Simard, M. Bouchard, and G. Lemire of UQAC, Dr M. Choquette of Université Laval, and P. Plamondon and J.-P. Masse of l'École Polytechnique de Montréal for their assistance in the microstructural examination.

References

1. Lloyd DJ (1997) In: Mallick PK (ed) Composites engineering handbook. Marcel Dekker, Inc, New York, p 631
2. Chen X-G (2006) In: Gupta N, Hunt WH (eds) Proceedings of TMS 2006, symposium on solidification processing of metal matrix composites, San Antonio, USA, March 2006, p 343
3. Flemings MC (1974) Solidification processing. McGraw-Hill Book Company, New York, p 219
4. Campbell J (1999) Casting. Butterworth Heinemanth, Oxford, p 75
5. Yarandi FM, Rohatgi PK, Ray S (1993) J Mater Eng Perform 2:359
6. Rohatgi P, Asthana R (2001) JOM 53:9
7. Surappa MK, Rohatgi PK (1981) Metal Mater Trans B 12B:327
8. Ravi VA, Frydrych DJ, Nagelberg AS (1994) AFS Trans 102:891
9. Kolsgaard A, Brusethaug S (1994) Mater Sci Tech 10:545
10. Ferguson J, Kemblowski Z (1991) Applied fluid rheology. Elsevier, London, p 199
11. Gourlay C, Laukli H, Dahle A (2004) Metal Mater Trans A 35A:2881
12. Laukli H, Lohne O, Arnberg L (2005) In: Tiryakioglu M, Crepeau PN (eds) Proceedings of TMS 2005, symposium on shape casting, San Francisco, USA, February 2005, p 263
13. Sannes S, Westengen H (1998) In: Mordike BL, Kainer KU (eds) Proceedings of magnesium alloys and their application, Wolfsburg, Germany, April 1998, p 223
14. Laukli H, Gourlay C, Dahle A, Lohne O (2005) Mater Sci Eng A 413–414:92
15. Zhang Z, Chen X-G, Charette A (2007) J Mater Sci 42:7354. doi:10.1007/s10853-007-1554-5
16. Dahle AK, St John DH (1999) Acta Mater 47:31
17. Chen X-G (2004) In: Proceedings of 14th international symposium on the packaging and transportation of radioactive materials, Berlin, Germany, 2004
18. Chen X-G (2005) In: Schlesinger ME (eds) EPD Congress 2005. TMS, San Francisco, USA, p 101
19. Viala JC, Bouix J, Gonzalez G, Esnouf C (1997) J Mater Sci 32:4559. doi:10.1023/A:1018625402103
20. Kennedy AR (2002) J Mater Sci 37:317. doi:10.1023/A:1013600328599
21. Pyzik AJ, Beaman DR (1995) J Am Ceram Soc 78:305

22. Shorowordi KM, Laoui T, Haseeb ASMA, Celis JP, Froyen L (2003) J Mater Process Tech 142:738
23. Zhang Z, Chen X-G, Charette A, Ghomashchi R (2005) In: Martin J-P (ed) Proceedings of light metals, Calgary, Canada, August 2005, p 447
24. Viala JC (2002) In: Drew RAL, Pugh MD, Brochu M (eds) Proceedings of the international symposium on metal/ceramic interactions, Montreal, Canada, August 2002, p 63
25. Gokhale AM (1990) In: Voort G (ed) ASM handbook, vol 9. The Materials Information Society, OH, p 431